Comput. Methods Appl. Mech. Engrg. 197 (2008) 4399–4410

Contents lists available at ScienceDirect

Comput. Methods Appl. Mech. Engrg.

journal homepage: www.elsevier.com/locate/cma

Design of microvascular flow networks using multi-objective genetic algorithms

Alejandro M. Aragón [a], Jessica K. Wayer [b], Philippe H. Geubelle [c,*], David E. Goldberg [d], Scott R. White [c]

[a] Department of Civil and Environmental Engineering, University of Illinois at Urbana-Champaign, 205 North Mathews Avenue, Urbana, IL 61801, USA
[b] Department of Aerospace Engineering, University of Illinois at Urbana-Champaign, 104 South Wright Street, Urbana, IL 61801, USA
[c] Beckman Institute of Advanced Science and Technology, University of Illinois at Urbana-Champaign, 405 North Mathews Avenue, Urbana, IL 61801, USA
[d] Illinois Genetic Algorithms Laboratory, University of Illinois at Urbana-Champaign, 104 South Mathews Avenue, Urbana, IL 61801, USA

ARTICLE INFO

Article history:
Received 30 January 2008
Accepted 13 May 2008
Available online 5 June 2008

Keywords:
Microvascular network
Genetic algorithms
Multi-objective optimization
Bio-mimetic material

ABSTRACT

A multi-objective genetic algorithm is used to design 2D and 3D microvascular networks embedded in bio-mimetic self-healing/self-cooling polymeric materials. Various objective functions and constraints are considered, ranging from flow efficiency and homogeneity to network redundancy and void volume fraction. The design variables include the network topology defined over a template and the microchannel diameters chosen among a finite set of values. The effect of network redundancy, template geometry and microchannel diameters on the Pareto-optimal fronts generated by the genetic algorithm is investigated.

1. Introduction

Inspired by vascular networks in living organisms, materials consisting of a network of microchannels embedded in a polymeric matrix offer great potential in various autonomic healing, cooling and sensing applications. One example of a bio-mimetic material uses hollow fibers embedded in a polymeric matrix and filled with an uncured healing agent, which is released when the fibers experience damage [13,23]. In a recent publication [35], Toohey and coworkers have demonstrated repeated healing of a polymer coating with the aid of a subsurface microvascular network containing a healing agent in monomeric form. As cracks form in the coating, the healing agent is wicked to the crack surfaces through capillarity and encounters solid catalyst particles contained in the coating. The healing process is thus initiated and can be repeated as long as the three-dimensional microvascular network contained in the polymeric substrate provides enough healing agent to the coating. The circulation of a liquid in the microvascular network is also being considered for thermal management of a structural component subjected to external thermal loading. An example of such an application can be found in [30] for the case of a microvascular network embedded in an epoxy matrix.

Interest in this class of bio-mimetic materials has also been driven by recent advances in manufacturing techniques such as the robotic deposition process, which allows for the creation of complex two- and three-dimensional microvascular network structures [34,38]. In this process, the microvascular network is drawn by extruding a fugitive ink on a polymer substrate through needle tips so that the resulting microchannels have diameters that can be as small as 10 μm. After the drawing process has taken place, the resulting structure is embedded in a liquid polymer that is subsequently cured. The ink contained within the polymer is then evacuated by heating the material, leaving the embedded microvascular network. The use of needle tips with different sizes and a fully automated nozzle with three-dimensional motion results in a powerful manufacturing methodology for the creation of complex patterns.

Various methods have been proposed in the literature for the design of flow networks, which presents a set of unique challenges in terms of the complexity of the objective functions, design variables and constraints. In the constructal theory [3], optimal flow structures are obtained by applying the constructal law, which states that the optimal flow structures should provide easier access to the flow than those that are non-optimal. This method has been used to optimize very simple geometries [4,19,39]. Another approach relies on topology optimization, which has been used primarily in structural design, but has been recently extended to the design of flow networks considered either as a continuum or as a discrete system [5]. A comprehensive study of flow networks using a discrete topology is given in [20], where the diameter variables are chosen from the positive real number set. Flow networks can also be designed by evolutionary algorithms, a family of biology-inspired methods that are increasingly gaining popularity because of their simplicity and applicability to the optimization of a large set of problems in numerous fields. Starting from a population of candidate solutions, evolutionary algorithms search for better candidates by applying a set of genetic operators and using a

* Corresponding author. Tel.: +1 217 244 7648; fax: +1 217 244 0720.
E-mail address: geubelle@uiuc.edu (P.H. Geubelle).

0045-7825/$ - see front matter © 2008 Elsevier B.V. All rights reserved.
doi:10.1016/j.cma.2008.05.025

function to differentiate those solutions that are more fit to solve the problem. The last twenty years have seen substantial progress in the understanding of the mechanics behind the optimization based on Genetic Algorithms (GAs) [15], the most popular of these evolutionary methods. GAs have been applied successfully to the optimization of flow networks over a wide range of objective functions [22,27,31,36].

The present study considers a discrete topology for the microchannels of the network and selects their diameters from a discrete set of values, in accordance to available tip sizes in the direct printing process mentioned earlier. For the optimization problems investigated in this work, a multi-objective genetic algorithm scheme is adopted for several reasons. First, the adopted GA can readily handle any number of objective functions in a unified formulation and accommodate the discrete nature of the design variables considered in the present study. Second, gradient-based search techniques may converge to a local optimum, while GAs search a much broader portion of the decision space and are thus more likely to yield a global optimum. Third, GAs can readily be hybridized with other search techniques [8], thus combining the robustness of the global evolutionary search with the accuracy of problem-specific local search methods. Finally, specific features of good solutions found in the GA optimization can be used to initialize another GA optimization (knowledge-based GAs).

The design of a microvascular network is application specific, so networks designed for flow efficiency may look very different from those designed for structural performance. Furthermore, when considering multiple objectives, there is a need to capture the tradeoff between those objectives in the form of an optimal front from which the network design can be readily selected. This optimal front must be extracted through analytical or computational means, by decomposing the problem into a set of conflicting objectives and constraints. This particular study focuses on the optimization of two- and three-dimensional simple geometries used in the manufacturing of bio-mimetic polymers. Whether the resulting polymer is used in self-healing or self-cooling applications, a fluid will be driven through the microchannels and flow efficiency is thus a key design objective. However, an optimal solution for the flow efficiency typically maximizes the void volume left by the network, so both objectives conflict with one another. Beyond these two primary objective functions, this paper also introduces objectives and constraints associated with flow homogeneity and network redundancy.

Section 2 introduces the problem to be solved and the formulation used to obtain the objective functions. Section 3 gives a brief introduction to multi-objective genetic algorithms. The results are presented in Section 4.

2. Problem description

The adopted mathematical model of a bio-mimetic material containing a microvascular network consists of two parts, as illustrated in Fig. 1 for a two-dimensional (2D) network. First, the bulk of the material is represented by a domain Ω (left Fig. 1) with area A (or volume V). Second, a graph data structure (right Fig. 1) is used to represent the microvascular network, where the $\mathscr{E}$ edges of the graph serve as network microchannels and the $\mathscr{V}$ vertices as possible locations for microchannel endpoints. The use of a graph data structure to represent the microvascular network allows us to take advantage of tools associated with graph theory [37]. A graph is *disconnected* if all vertices are not reachable from each other through the existing edges. Another important concept borrowed from graph theory is the *degree* of a vertex, d, defined as its number of incident edges. This parameter is used to constrain the optimization in order to ensure complete network coverage of the domain and also to investigate the reliability of the network when subjected to damage, as explained in Section 2.3.

The current study focuses on convex domain geometries, namely a rectangle in 2D and a cuboid in 3D. We denote by a and b the sides of a rectangular 2D domain and by a, b and c the lengths of the edges of a 3D cuboid. Since there is an infinite number of possible network configurations that fit within the domain boundary, we restrict the number of possible vertex locations to a set of points located over an N-dimensional lattice,

$$\Lambda = \left\{ \sum_{i=1}^{N} z_i \mathbf{e}_i \mid z_i \in \mathbb{Z} \right\}, \quad \Lambda \subset \Omega,$$

where the basis vectors for the Euclidian space $\mathbb{E}^N$ have equal magnitude in all directions $\|\mathbf{e}_i\| = \delta$. In other words, the possible vertex locations are limited to the intersection vertices of a regular Cartesian grid having grid spacing δ, such that two neighboring vertices on any Cartesian axis direction are separated by a constant distance. The vertices of the graph data structure corresponding to the point lattice are shown as open circles in the right figure. Similarly, the number of possible edges is limited to those connecting neighboring vertices. With these simplifications, the number of possible network configurations is drastically reduced. Several properties are assigned to the graph data structure that represents the microvascular network. A coordinate property in $\mathbb{E}^N$ is associated with each

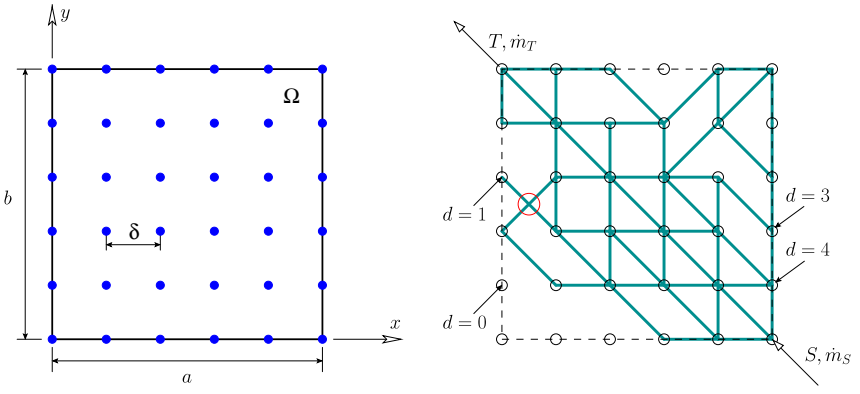

Fig. 1. Bio-mimetic material mathematical model. The left figure shows the domain Ω and the 2D point lattice spanned over Cartesian coordinates. The graph data structure that represents the microvascular network is shown on the right. Vertices of the graph laying on top of the 2D point lattice, marked as circles, represent possible microchannel endpoints whereas edges of the graph represent the actual microchannels. Examples of flow boundary conditions (inflow S and outflow T locations), together with examples of vertex degrees d are also included.

vertex corresponding to a point in the lattice. Each edge represents a cylindrical microchannel and has a length L and diameter D. Networks containing microchannels oriented only in the directions of the coordinate axes will be henceforth referred to as *orthogonal*. Similarly, we will refer to as *diagonal* those networks having diagonal microchannels in addition to the orthogonal ones (right Fig. 1).

The optimization process starts from an initial structure that we call the *template network*, which is the equivalent to the ground structure used in topology optimization [20]. This template network has the maximum number of edges for the type of networks being designed, and is illustrated in Fig. 2 for orthogonal and diagonal networks over a 6×6 point lattice. The optimization then consists in finding the diameter for each edge of the template structure from a finite set of discrete values $\mathscr{D} = \{D_0, D_1, \ldots, D_m\}$ such that the resulting networks minimize two or more objective functions subjected to a set of constraints. In contrast to the preliminary study on orthogonal networks presented in [1], the present study also allows for diagonal microchannels. However, microchannels are permitted to intersect only at locations determined by the spatial point lattice in the optimization process, so that a network containing microchannels intersecting outside the point lattice (large hollow circle in Fig. 1) is marked as unfeasible.

The solution of the flow objective functions requires boundary conditions. Fig. 1 shows the inflow and outflow vertices located at the lower-right and upper-left corners of the domain, respectively. These are the boundary conditions considered in the 2D problems investigated in this work, although other configurations including multiple inflows and outflows can also be considered. The formulation used to obtain the objective functions and constraints is described next.

2.1. Void volume fraction and intersection constraint

The presence of a microvascular network in a material can have a detrimental impact on its response to external loads as it tends to decrease its stiffness and strength. Thus, one of the requirements for these materials is to minimize the void volume associated with the microvascular network. For a 2D domain, the void volume fraction is defined as

$$v = \frac{\sum_{i=1}^{\mathscr{E}} L_i D_i}{A}, \tag{1}$$

corresponding to the normalized projected area of the network over its plane. Note that this definition does not correct for the overlapping areas between adjacent microchannels, which is assumed to be negligible for microchannels with high aspect ratios. Similarly, for 3D domains and cylindrical microchannels, the void volume fraction is defined as

$$v = \frac{\pi \sum_{i=1}^{\mathscr{E}} L_i D_i^2}{4V}. \tag{2}$$

When dealing with the optimization of diagonal network templates, there exists the possibility of producing networks where microchannels intersect at locations other than those determined by the point lattice. As mentioned earlier, these networks are considered to be unfeasible. Furthermore, the flow pressure values described in the next section are computed only at lattice point locations so the pressure drop resulting from those unfeasible networks is incorrect. Even though this problem could be avoided by creating a vertex at the microchannel intersection, it may be desirable from the manufacturing point of view to have the microchannels intersect at points determined by the point lattice. We thus introduce the microchannel intersection constraint, g_I, as

$$g_I = \sum_{i=1}^{\mathscr{E}} \sum_{j=1,\ j\neq i}^{\mathscr{E}} \eta_{ij}^I, \tag{3}$$

where $\eta_{ij}^I = 1$ if microchannels i and j intersect at a location not determined by the lattice and $\eta_{ij}^I = 0$ otherwise.

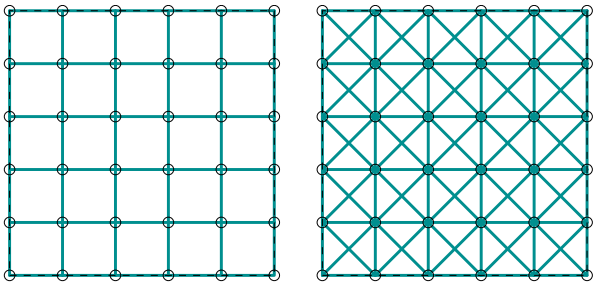

Fig. 2. 2D template structures for orthogonal (left) and diagonal (right) networks.

2.2. Flow efficiency and constraints

The flow efficiency is obtained by computing the maximum pressure drop between any two vertices in the spatial domain, assuming that the pressure drop in any microchannel i is given by the classical Hagen-Poiseuille law

$$\Delta p_i = \frac{128 \nu L_i}{\pi D_i^4} \dot{m}_i, \tag{4}$$

where ν and $\dot{m}_i$ denote the kinematic viscosity and mass flow rate of the fluid, respectively. Assembling the contribution of all microchannels in the network results in a linear system of equations $\vec{K}\vec{p} = \vec{c}$, where $\vec{K}$ is the network characteristic matrix, $\vec{p}$ is the network pressure vector and $\vec{c}$ is the network consumption vector [6]. Boundary conditions for this problem involve prescribed pressure values at outflow locations and prescribed flow at the inflow. The flow efficiency of the network is thus quantified by

$$\Delta p = \max_{i,j=1}^{\mathscr{N}} |p_i - p_j|. \tag{5}$$

Note that the pressure drop in a microchannel (Eq. (4)) is inversely proportional to the fourth power of its diameter, in contrast to the linear or quadratic relationship found earlier for the void volume fraction (Eqs. (1) and (2)).

A good microvascular network design not only minimizes the energy needed to drive the flow through the network but also ensures that each of the microchannels has an active flow. This is particularly important for self-cooling or self-sensing applications. Thus, inner loops with no pressure differential have to be eliminated from the optimization, but the GA cannot infer this information from the pressure drop computation given earlier. As a result, we label as unfeasible those networks where there is zero flow in at least one of their microchannels. To that purpose, we define the non-zero flow constraint, g_F, as

$$g_F = \sum_{i=1}^{\mathscr{E}} \eta_i^F, \quad \eta_i^F = \begin{cases} 1 & \text{if } \dot{m}_i = 0, \\ 0 & \text{otherwise.} \end{cases} \tag{6}$$

When dealing with multiple targets, there is a need to distribute the outflow evenly among the various targets. Consider that the resulting design of a square microvascular network is just a cell of a larger structure. Certainly, outflows that share a boundary of the network will become inflows for a contiguous cell, so having heterogeneous flows will introduce another complexity in the design of contiguous cells. On the other hand, if the healing process is started at outflow locations (as in the healing of a coating [35]), flow homogenization is also needed to obtain homogeneous healing. The fluid healing agent undergoes a chemical reaction with the catalyst that is present in the coating, but this reaction could be avoided completely if the flow were too high (washed out) or it

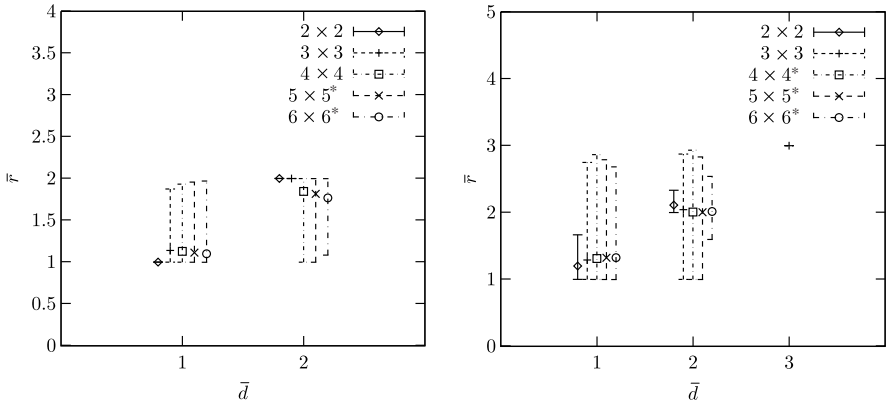

Fig. 3. Correlation between the minimum degree $\bar{d}$ and average network redundancy $\bar{r}$ (Eq. (9)) for orthogonal (left) and diagonal (right) networks of various lattice sizes. For each data set, the average value of $\bar{r}$ for the survey is marked along with error bars indicating minimum and maximum values. An asterisk indicates that the data was obtained through sampling.

could even block the outflow if the flow were too low. To ensure that the healing process at the T outflow locations be as homogeneous as possible, we define the flow homogeneity parameter, ζ, as

$$\zeta = \frac{1}{\dot{m}_S} \max_{i,j=1}^{T} |\dot{m}_i - \dot{m}_j|, \tag{7}$$

where the maximum outflow difference is normalized by the total network inflow.

2.3. Coverage and redundancy

In the case of self-healing polymers, an ideal microvascular network will cover the entire domain so that internal cracks nucleating anywhere in the domain can be arrested before reaching a critical length leading to a catastrophic failure. The coverage is hereafter imposed as a constraint by simply requiring a minimum degree $\bar{d}$ on each vertex of the graph that represents the microvascular network. The degree constraint, g_D, is then computed as

$$g_D = \sum_{i=1}^{\mathscr{V}} \eta_i^D, \quad \eta_i^D = \begin{cases} 1 & \text{if } d_i < \bar{d}, \\ 0 & \text{otherwise.} \end{cases} \tag{8}$$

Probably the most desirable feature in the design of a microvascular network for self-healing applications is the reliability of its structure when subjected to damage. In other words, when one or more microchannels are cut within the domain, the healing agent must be able to reach most if not all areas in a good network design. The severity of such a cut depends on the location of the damaged microchannels, ranging from preventing flow to a single vertex in a corner to completely preventing any vertex from receiving flow (in case the microchannel connecting the inflow is cut). This problem has been studied thoroughly in the literature and is designated as the *survivable network design problem* [24,33]. The reliability of a network is obtained numerically through the redundancy matrix $\mathbf{r}$, where each entry r_{ij} represents the number of *node disjoint paths*[1] between the ith and jth vertices. In other words, r_{ij} denotes the number of microchannels that have to be damaged in order to make vertex j unreachable from vertex i. It is well known that the redundancy matrix can be obtained by solving the maximum flow problem after assigning a unit capacity to all edges [24]. However, obtaining the redundancy matrix is computationally expensive since each entry r_{ij} has a complexity $\mathscr{O}(\mathscr{V}\mathscr{E}^2)$ with the algorithm devised by Edmonds and Karp [11]. Since the computation of the minimum degree $\bar{d}$ is only of complexity $\mathscr{O}(\mathscr{V})$, we have opted to investigate the relation between this parameter and the resulting network redundancy.[2] We use the observation that there must be at least $\bar{d}$ incident microchannels between vertices i and j if there are to be $\bar{d}$ disjoint paths between them. Nevertheless, this is just a necessary condition since r_{ij} might be lower than $\bar{d}$ even if both vertices have $\bar{d}$ incident microchannels.

To support this statement, let us consider the two groups of 2D networks considered in this study over a square domain, i.e., the orthogonal and diagonal microvascular networks. Furthermore, let us use the diameter set $\mathscr{D} = \{0, 1\}$ to indicate the presence or absence of a microchannel in the network. Both the dimensions of the domain and the magnitude of the diameters used are irrelevant to this study, which aims at correlating the redundancy of the network to its minimum degree. In any cartesian direction, there are $n = a/\delta + 1$ vertex locations. For a particular value of n, there are a total of $|\mathscr{D}|^{\mathscr{E}}$ possible microvascular networks, with $|\mathscr{D}| = 2$, $\mathscr{E} = n(n-1)$ for orthogonal networks and $\mathscr{E} = 2(2n-1)(n-1)$ for diagonal networks. The lattices considered range from 2×2 up to 6×6. It is clear that the exponential dependence on the number of edges, which in turn depends on n, makes the study of larger lattices prohibitively expensive. Note on the other hand that many of the networks within that total are not considered because they are either disconnected networks or, in the case of diagonal networks, there are microchannels that intersect in points not defined by the 2D lattice. Since the redundancy matrix is symmetric (i.e., $r_{ij} = r_{ji}$), let us define the network average redundancy as

$$\bar{r} = \frac{2}{\mathscr{V}(\mathscr{V}-1)} \sum_{i=1}^{\mathscr{V}} \sum_{j=i+1}^{\mathscr{V}} r_{ij}. \tag{9}$$

Fig. 3 shows the average redundancy values for the feasible orthogonal (left) and diagonal (right) networks, where each data set includes only structures for a particular lattice size. For each set, the average of $\bar{r}$ over all networks in the survey is marked by a symbol, along with error bars that indicate maximum and minimum values. Results are slightly offset along the $\bar{d}$ axis to ease the visualization. For orthogonal networks (left Fig. 3), a 5×5 lattice requires more than a trillion evaluations. As a result, a sample of the total number of networks was taken for the evaluations (indicated in the figures by an asterisk after the lattice size). The sampling size, ranging from

[1] Two paths are called disjoint if they share no nodes other than the endpoints [33].

[2] The definition of $\bar{d}$ is in contrast to the formal definition of the degree of a graph, which is the maximum degree of its vertices.

10^6 to 10^7 networks, was increased until no significant variation was obtained in the results. For diagonal networks (right Fig. 3), a sampling was required even for a 4×4 lattice since a complete survey of all networks involves more than 4 trillion evaluations. The figures show a quasi linear dependence between the minimum degree of a network and its average reliability. In other words, a microvascular network with minimum degree $\bar{d}$ has a high probability of having $\bar{r} = \bar{d}$. This allows us to use the degree as a fundamental parameter in the design of microvascular networks.

3. Genetic algorithms

Since their introduction more than four decades ago [16,17], GAs have proven to be an efficient heuristics tool for the optimization of complex design problems. The notation adopted in this section follows the convention used in [2,29]. GAs usually start the optimization from a population $\mathscr{P}$ containing a fixed number $|\mathscr{P}|$ of individuals $\mathscr{I}$, each with a distinctive chromosome $\mathscr{C}$. In order to use the algorithm, a suitable representation must be chosen to encode in the chromosome of an individual the different characteristics of the problem for which an optimum is sought. The chromosome is a numeric string where each location (allele $\mathscr{A}$ in GA terminology) encodes a parameter (or part of it) of the problem. The alleles can be chosen from a binary alphabet ($\mathscr{A}_i \in \{0,1\}$), a k-ary alphabet ($\mathscr{A}_i \in \{0,1,\ldots,k-1\}$), or from the real numbers ($\mathscr{A}_i \in \mathbb{R}$).

In a simple GA [14], the population of individuals $\mathscr{P}_0$ is initialized randomly, after which the algorithm enters a loop over $t_{\max}$ iterations or generations. In this loop, the entire population is first evaluated according to a prescribed objective function that describes numerically how fit the individuals are to solve the problem at hand. After this step another loop is initiated to determine the parent population for the next generation by applying the genetic operators *selection*, *crossover* and *mutation*. The selection mechanism is where the "survival of the fittest" takes place since those individuals that are more fit are more likely to be selected for reproduction. The mixing of the genetic information takes place in the crossover operator, where two selected individuals interchange the alleles of their chromosomes according to a certain criterion. The mutation is a slight modification in the characteristics of an individual and it is usually performed by changing the value of one of the alleles in the chromosome.

Even though the simple GA can be used to solve multi-objective optimization problems (MOOPs) [28], better results can be achieved by using multi-objective evolutionary algorithms (MOEAs) [18,32,12,21]. With the simple GA, a MOOP is converted to a single weighted objective function, with different weights selected to assign different priorities to the corresponding objectives. The drawbacks of using a simple GA to solve MOOPs are evident not only because the solution obtained cannot capture the tradeoff between the different objectives but also because the determination of the weighting factors tends to influence the solution substantially. MOEAs, on the other hand, can capture the tradeoffs between conflicting objectives by carrying out a Pareto-optimization, in which individuals are compared in all objectives to determine the best candidates for the next generation. Some definitions are needed to understand how the MOEA-based optimization process works. At a given generation $t < t_{\max}$, let us divide the population in two mutually exclusive sets containing feasible and unfeasible individuals, i.e.,

$$\mathscr{P} = \mathscr{P}^{\mathrm{F}} \cup \mathscr{P}^{u}, \quad \mathscr{P}^{\mathrm{F}} \cap \mathscr{P}^{u} = \emptyset,$$

where $\mathscr{P}^{\mathrm{F}} = \{\mathscr{I}_i | \mathbf{g}_i = \mathbf{0}\}$ and $\mathscr{P}^{u} = \{\mathscr{I}_i | \mathbf{g}_i \neq \mathbf{0}\}$. Let the domination operator, $\ll_{\mathscr{S}}$, over the space $\mathscr{S}$ be defined such that the ith individual $\mathscr{I}_i$ in the population $\mathscr{P}$ dominates another individual $\mathscr{I}_j$ if $\mathscr{I}_i$ is better than $\mathscr{I}_j$ in at least one dimension over the space $\mathscr{S}$ and is no worse in the rest.[3] Therefore, we denote $\mathscr{I}_i \ll_{\mathscr{G}} \mathscr{I}_j$ an individual $\mathscr{I}_i$ that dominates another individual $\mathscr{I}_j$ in the constraint function space $\mathscr{G}$. The same reasoning follows for the objective function space $\mathscr{F}$. With this definition, let the global domination operator, $\lll$, be defined such that $\mathscr{I}_i$ dominates $\mathscr{I}_j$ (i.e., $\mathscr{I}_i \lll \mathscr{I}_j$) if any of the following conditions holds:

- $\mathscr{I}_i \in \mathscr{P}^{\mathrm{F}}, \mathscr{I}_j \in \mathscr{P}^{u}$.
- $\mathscr{I}_i, \mathscr{I}_j \in \mathscr{P}^{u}, \mathscr{I}_i \ll_{\mathscr{G}} \mathscr{I}_j$.
- $\mathscr{I}_i, \mathscr{I}_j \in \mathscr{P}^{\mathrm{F}}, \mathscr{I}_i \ll_{\mathscr{F}} \mathscr{I}_j$.

In other words, the ith individual dominates the jth individual if $\mathscr{I}_i$ is feasible and $\mathscr{I}_j$ is not, or both individuals are unfeasible but $\mathscr{I}_i$ dominates $\mathscr{I}_j$ in constraint function space $\mathscr{G}$, or both individuals are feasible and $\mathscr{I}_i$ dominates $\mathscr{I}_j$ in objective function space $\mathscr{F}$. With this definition, the evolution is different from a single-objective optimization since the selection process keeps nondominated solutions. This is schematically shown in Fig. 4, where a randomly created population is optimized[4] for two objective functions ϕ_1 and ϕ_2. Through the evolution process, all individuals approach the so-called Pareto-optimal front, where all individuals lying on it are optimal solutions to the MOOP.

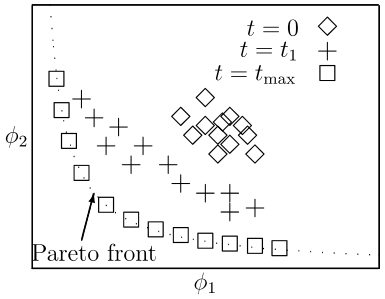

Fig. 4. Schematic of multi-objective optimization, showing a randomly created population of individuals at $t = 0$ evolving towards a Pareto-optimal front at iteration $t = t_{\max}$.

For this work, the Non-dominated Sorting Genetic Algorithm II (NSGA-II) introduced by Deb et al. [10] is used. The original algorithm was modified in order to handle constraints by using the operator $\lll$ defined earlier, and is described in Algorithm 1.

Algorithm 1. NSGA-II [10]

procedure Evolve ($|\mathscr{P}|, t_{\max}$)
  $\mathscr{P}_0 = random(|\mathscr{P}|)$
  $Q_0 = apply\text{-}genetic\text{-}operators(\mathscr{P}_0)$
  while $t < t_{\max}$ **do**
    $t \leftarrow t + 1$
    $R_t = \mathscr{P}_t \cup Q_t$
    $F = fast\text{-}nondominated\text{-}sort(R_t)$
    repeat
      $crowding\text{-}distance\text{-}assignment(F_i)$
      $\mathscr{P}_{t+1} = \mathscr{P}_{t+1} \cup F_i$
    until $|\mathscr{P}_{t+1}| < |\mathscr{P}|$
    sort($\mathscr{P}_{t+1}, \lll$)
    $\mathscr{P}_{t+1} = \mathscr{P}_{t+1}[0 : |\mathscr{P}|]$
    $Q_{t+1} = apply\text{-}genetic\text{-}operators(\mathscr{P}_{t+1})$
  end while
end procedure

[3] The concept of dominance is borrowed from the field of economics and it is due to Vilfredo Pareto [25].

[4] Minimization is carried out in the schematic figure, thus the Pareto-optimal front is closer to the origin at the lower-left corner.

The main difference between the simple GA and the NSGA-II presented in Algorithm 1 is in the way individuals are selected in order to retain those nondominated solutions. An offspring population is obtained by applying the same genetic operators used for the simple GA, forming a combined parent-offspring population of size $2|\mathscr{P}|$. All individuals in the combined population are grouped first according to their non-domination rank in fronts F_i, $i = 1,2,\ldots,n$, such that individuals in F_i dominate those of subsequent fronts (i.e., fronts F_j, $j > i$). In order to select the individuals that will constitute the parent population in the next generation, the algorithm first selects all fronts that completely fit in the population size (i.e., all fronts F_i are selected such that $|\cup_i F_i| \leqslant |\mathscr{P}|$). The $|\mathscr{P}| - |\cup_i F_i|$ remaining individuals (if any) are selected by also considering a crowding parameter, used to distribute individuals more evenly along the fronts throughout the computation. To illustrate how the algorithm works, consider the two-objective optimization problem MPO4 presented in [10]. The left plot in Fig. 5 shows the 100 selected individuals, most of them lying in the Pareto-optimal front for this problem, while the right plot presents the resulting fronts obtained in that particular generation for the combined population of size $2|\mathscr{P}|$. Note that, on the figure that shows the fronts F_i, the discrete points are joined by lines for visualization purposes, but the lines themselves do not represent the fronts.

3.1. Microvascular network representation

As mentioned earlier, the use of GAs to carry out the optimization of a problem involves finding a suitable GA representation. In our case, the microvascular network is idealized as a graph data structure and the optimization is carried out on the diameters. An integer representation of cardinality k, referred to as k-ary alphabet in GA terminology, is chosen to represent the set of k possible discrete diameters. Therefore, the number of alleles in the chromosome of a *network individual* equals the number of microchannels in the network and the allele values map to a discrete set of diameters, chosen according to manufacturing requirements.

To illustrate the network representation, let us consider a 2D diagonal network template on a 3×3 point lattice (left Fig. 6). This template has 20 microchannels and a conforming chromosome will have the same number of alleles. Let the possible diameter choices be limited to the set $\mathscr{D} = \{D_i | D_i = i \cdot 25\ \mu\text{m}, i = 0,1,\ldots,5\}$. Then, the chromosome

$$\mathscr{C} = \{44031205311400225042\}$$

produces the mapping shown at the right in Fig. 6, i.e., the first and second alleles map to a diameter $D_4 = 100\ \mu$m, the third one maps to $D_0 = 0\ \mu$m (absence of the microchannel), the fourth one to $D_3 = 75\ \mu$m, and so forth.

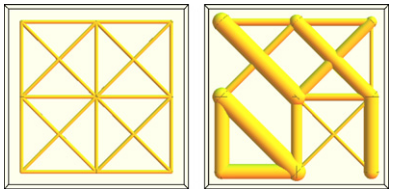

Fig. 6. Network template (left) for diagonal networks over a 3×3 point lattice and resulting microvascular network (right) after applying the mapping given by a chromosome $\mathscr{C}$.

3.2. Objective functions and constraints

The selection process within the GA needs to differentiate the "fittest individuals" by assigning numerical values to each of the objective functions and constraints considered. Most of the study presented in this manuscript focuses on the objective functions associated with the flow efficiency and void volume fraction, with an example considering also the flow homogeneity across outflow locations. The coverage of the network is imposed by constraint, as well as the requirement to have intersection of microchannels only at lattice point locations. Most examples will also enforce the presence of flow in every microchannel. In all cases presented in this paper, the optimization involves the minimization of the objective functions and is stated formally as

$$\begin{aligned} &\text{minimize} \quad \{\phi_i\}_{i=1}^{P}, \\ &\text{such that} \quad \{g_j\}_{j=1}^{Q} = \mathbf{0}, \end{aligned} \tag{10}$$

where the optimization is carried out on the set of P objective functions subjected to Q equality constraints.

The void volume fraction is computed using Eqs. (1) and (2) for the 2D and 3D networks, respectively. The flow efficiency is evaluated through the computation of the maximum pressure difference between any two vertices of the network, i.e., Eq. (5). The computed values are normalized by a reference network topology. For 2D problems involving a square domain of side a with a single inflow and outflow located at opposite corners (right Fig. 1), the reference network consists of a single microchannel connecting the source to the target with diameter $D_{\text{ref}} = 100\ \mu$m. The corresponding reference values for the void volume fraction (v_{ref}) and pressure drop (Δp_{ref}) are

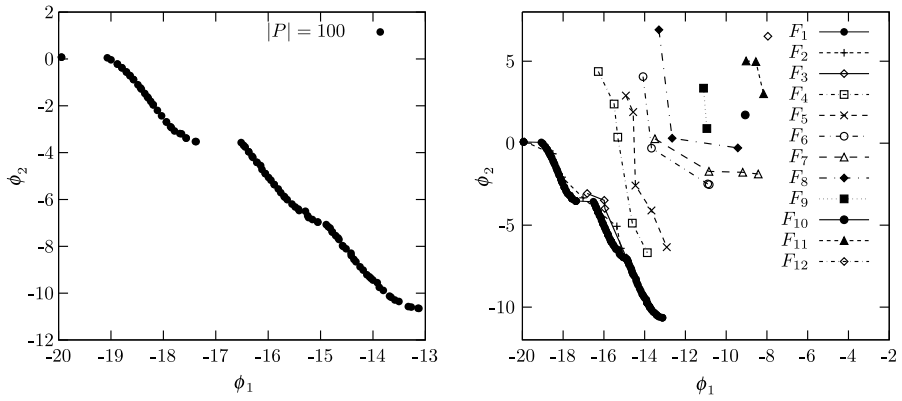

Fig. 5. NSGA-II results for problem MPO4 [10] at a particular generation, showing most individuals lying on the Pareto-optimal front for this problem (left) and the corresponding non-dominated fronts F_i, $i = 1,\ldots,12$ (right). Discrete points representing the fronts in the right figure are joined by lines for visualization.

$$v_{\text{ref}} = \frac{\sqrt{2}D_{\text{ref}}}{a}, \quad \Delta p_{\text{ref}} = \frac{128\sqrt{2}a\nu}{\pi D_{\text{ref}}^4}\dot{m}_S. \tag{11}$$

For more complex 3D problems with single or multiple outflow locations, the reference network topology is chosen to be the same as the template used in the optimization, with a reference diameter D_{ref}.

Thus, the objective functions associated with the void volume fraction (ϕ_v) and flow efficiency (ϕ_f) are

$$\phi_v = \frac{v}{v_{\text{ref}}}, \quad \phi_f = \frac{\Delta p}{\Delta p_{\text{ref}}}, \tag{12}$$

where v and Δp correspond to the values of the network being evaluated. A third objective function considered in this study is the flow homogeneity defined by Eq. (7) (i.e., $\phi_h = \zeta$), where the maximum flow difference among outflows is normalized by the total inflow. Since zero diameter (i.e., missing) channels are considered in the optimization process, disconnected networks may occur. Where such a network is found, very high values are assigned to ϕ_f and ϕ_h so the network becomes a "bad individual" for the selection process in the GA.

3.3. Genetic operators

The creation of an offspring population in the NSGA-II algorithm to form the combined population involves the use of genetic operators. For the selection process, tournament selection with selection pressure $s = 4$ is used [15]. In tournament selection, two individuals are selected and the dominated individual according to the operator $\lll$ defined in Section 3 is discarded. The winner is then compared to another contender and this process is repeated until s individuals are compared.

One point crossover is used in all crossover operations [14]. This mechanism randomly selects one of the $|\mathscr{C}| - 1$ possible crossover points and then exchange all alleles between the two selected individuals after this point. A high probability of crossover p_c is used in this work, usually $p_c = 0.9$.

The chromosomes in this study have cardinality $k > 2$ so simple bit mutation, the most common mutation operator [14], cannot be used. The mutation operator considered here uses a Gaussian probability density function centered at the value of the allele to be mutated. In this way, the mutation has a higher probability to select values that are close to the original allele. This technique is borrowed from other evolutionary algorithms and is adapted so it can be used with integer values. The probability of mutation p_m is chosen such that, on average, at most one allele is mutated in the chromosome, i.e., $p_m \leqslant 1/|\mathscr{C}|$.

4. Results

This section starts with the description of a typical multi-objective optimization using GAs, followed by a series of optimized problems. If not explicitly stated, it is implied that the GA has completely converged to a Pareto-optimal front. This can be concluded after observing no significant differences on the front for many generations.

4.1. Multi-objective constrained optimization

To illustrate the optimization process, consider a 2D square domain with side $a = 10$ mm where the point lattice has $\delta = 1$ mm (11×11 lattice), resulting in $\mathscr{V} = n^2 = 121$ vertex locations, with $n = a/\delta + 1$. The set of possible diameter choices is $\mathscr{D}[\mu\text{m}] = \{0, 100, 200\}$. The inflow and outflow vertices are located in the lower-right and upper-left corners, respectively. A diagonal template is considered for the optimization, containing $\mathscr{E} = 2(2n-1)(n-1) = 420$ edges. We constrain the optimization to those networks having microchannel intersections at lattice point locations (Eq. (3)), covering the entire domain with a minimum degree $\bar{d} = 2$ (Eq. (8)) and with flow at every microchannel (Eq. (6)). Considering as objectives for the optimization the void volume fraction and the flow efficiency, the resulting optimization problem is stated as

$$\begin{aligned} &\text{minimize} \quad \boldsymbol{\phi} = \{\phi_v, \phi_f\}, \\ &\text{such that} \quad \mathbf{g} = \{g_D, g_I, g_F\} = \mathbf{0}. \end{aligned}$$

A typical run of the multi-objective optimization is illustrated in Fig. 7, which present snapshots of the objective function and constraint spaces at generations $t = 0$, $t = 21$ and $t = 25$. The initial randomly generated population contains only unfeasible individuals, as shown in Figs. 7a and d. Both plots show only those individuals for

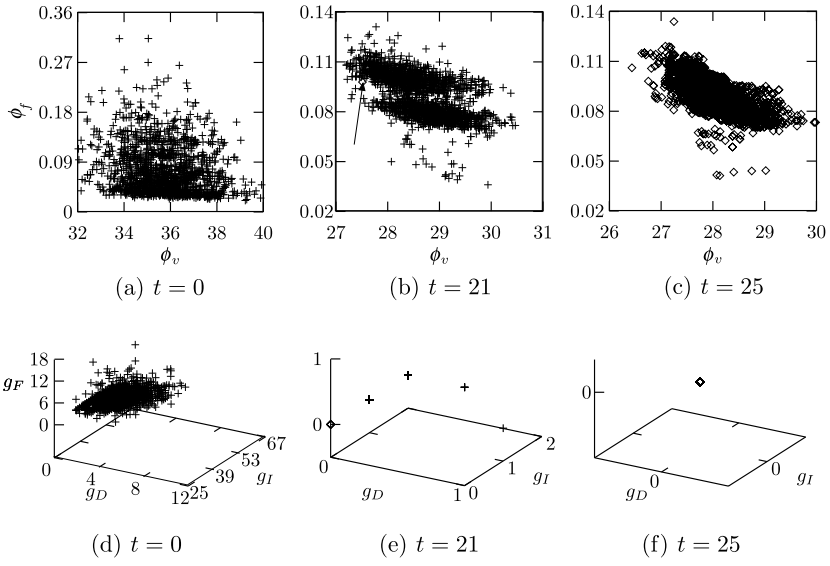

Fig. 7. Objective function and constraint spaces at three early steps of the optimization ($t = 0$, $t = 21$ and $t = 25$). Plots on the upper row show the objective function space composed of void volume fraction ϕ_v and flow efficiency ϕ_f. Plots on the lower row show the constraint function space, composed of degree constraint g_D, intersection constraint g_I and flow constraint g_F. Crosses (+) and diamond ($\diamond$) symbols indicate unfeasible and feasible individuals, respectively.

which the microvascular network is not disconnected, accounting for approximately 71% of the total. Recall that when a disconnected network is found, the flow efficiency objective and the non-zero flow constraint are penalized with a very high value (i.e., machine representation of infinity). At this stage the optimization is carried out in constraint space and the algorithm selects the better structures for the next generation according to their feasibility. Generation $t = 21$ is the first generation for which a feasible individual appears (indicated by an arrow in Fig. 7b) and the entire population becomes feasible after only four more generations as shown in Figs. 7c and f. After this point, the optimization is carried out in objective function space until the algorithm converges to the Pareto-optimal front. It is worth mentioning that unfeasible individuals are completely eliminated from the population after a few generations for all objective functions and constraints presented in this work. Moreover, no new unfeasible solutions appear after the entire population becomes feasible.

Optimization results after 2000 generations for a population size $|\mathscr{P}| = 5000$ are presented in Fig. 8 (top). The obtained Pareto-optimal front for competing objectives ϕ_v and ϕ_f is shown on the left, whereas the microvascular networks for selected individuals labeled (a) through (d) are shown on the right. Individual (a), which is composed only of 100 μm diameter microchannels, has the minimum void volume fraction but the highest pressure drop. Individual (b) shows a set of connected microchannels with the largest diameter $D = 200$ μm directing most of the flow through a direct path between the source and the target. The emergence of this path in the solution creates a jump in the flow efficiency in the Pareto-optimal front. Similarly, the network corresponding to individual (c) has three main paths of microchannels with the largest diameter. Finally, individual (d) is the right-most individual resulting from this particular optimization, having the maximum void volume fraction, but the minimum pressure drop. It is important to note that all the networks obtained in this optimization are optimal solutions to the problem and that all of them respect the imposed constraints. Moreover, the algorithm picks the best orientation for most of the diagonal microchannels in the resulting optimized structures even though the starting template structure is not biased regarding the orientation.

Constraints reduce the search space and guide the GA to obtain only networks with desired properties and/or without undesired features. For example, consider the same optimization problem subjected this time to constraints $\mathbf{g} = \{g_D, g_I\}$, i.e., without the non-zero flow constraint. The results for this optimization are illustrated in Fig. 8 (bottom), where the darker-colored microchannels of the selected networks correspond to those that have no flow. In fact, for this particular run 90% of the resulting optimized structures had microchannels with zero flow. Interestingly, the Pareto-optimal front in this optimization is almost identical to that obtained while accounting for the non-zero flow constraint (top-left Fig. 8), but the resulting structures have a completely different behavior.

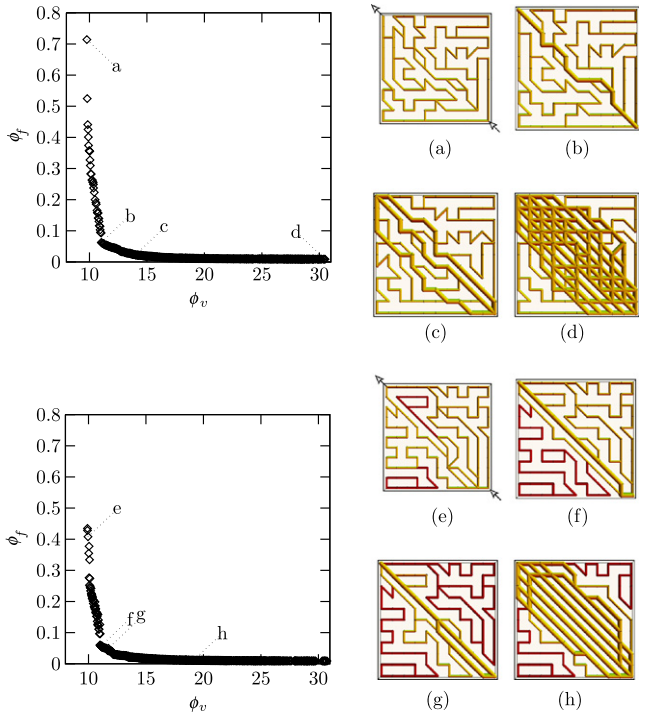

Fig. 8. Pareto-optimal front and selected networks after 2000 generations for a 11×11 square lattice with $\bar{d} = 2$, considering non-zero flow constraint (top), and neglecting it (bottom). Inflow and outflow vertices are located in the lower-right and upper-left corners, respectively (denoted by arrows in Figs. 8a and e). Eight networks labeled (a) through (h) on the optimal fronts are shown on the right. The darker segments in networks (e) through (h) denote microchannels with zero flow.

4.2. Effect of microchannel orientation

The effect of the microchannel orientation is studied here by comparing the optimization of an orthogonal network template (left Fig. 2) with the fully constrained results of the previous section. Thus, the optimization of the orthogonal template uses the same domain size and point lattice described earlier (i.e., $a = 10$ mm, $\mathscr{V} = n^2 = 121$ vertex locations, $n = a/\delta + 1$). Void volume fraction and flow efficiency are used again as the objective functions. The orthogonal template has a total of $\mathscr{E} = 2\,n(n-1) = 220$ edges and is optimized using the diameter set $\mathscr{D}_O[\mu\text{m}] = \{100, 200\}$. There is no need to constrain this optimization because the absence of the null diameter ensures complete coverage and intersections only occur at lattice points. Therefore, the optimization of the orthogonal template is stated as

$$\text{minimize} \quad \boldsymbol{\phi} = \{\phi_v, \phi_f\}.$$

Recall from the previous section that the diagonal template considers also the null diameter, allowing for a possible match between the resulting diagonal and orthogonal networks in certain areas of the domain.

The NSGA-II results for both optimization problems are plotted in Fig. 9, where they are denoted as *orthogonal* and *diagonal*. Different population sizes and maximum number of generations were chosen for each optimization. The chromosome size and its cardinality (number of possible allele choices) are higher for diagonal

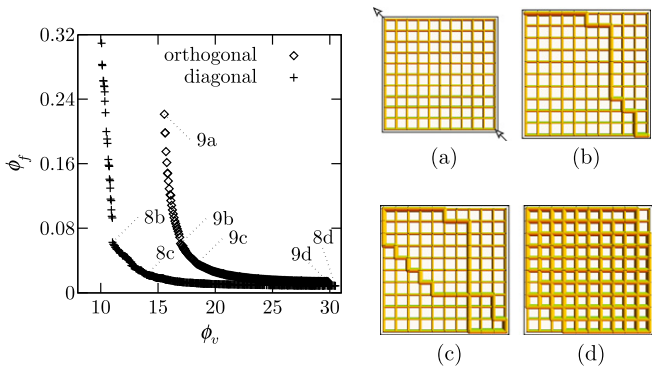

Fig. 9. NSGA-II results for the optimization of orthogonal and diagonal network templates (left) and selected microvascular networks for the orthogonal template optimization (right). Refer to Figs. 8b through 8d for selected diagonal networks. Fig. 9a shows the inflow and outflow locations.

networks, so the genetic algorithm needs more computational resources to obtain solutions lying on the Pareto-optimal front. The optimization of orthogonal networks was run for 1000 generations with a population size $|\mathscr{P}| = 3000$. The orthogonal data set shows the entire population on the Pareto-optimal front. Recall from the previous section that the optimization of the diagonal network was run for 2000 generations with a population size $|\mathscr{P}| = 5000$. Not all the individuals of the diagonal data set are displayed as the figure is cropped for visualization purposes.

Four networks from the orthogonal template optimization, labeled (a) through (d) on the Pareto-optimal front, are selected for visualization (right Fig. 9). Labels Figs. 8b through 8d refer to the diagonal networks presented in Fig. 8 for the fully constrained optimization. As in the previous section, Fig. 9a corresponds to the individual with the minimum void volume fraction but with the highest flow resistance. All the microchannels in the microvascular network converged to the minimum value $D = 100$ μm. Solutions in Figs. 9b and c resemble those given in the previous section, where most of the flow is directed through main paths of interconnected microchannels having the largest diameter. An individual for which almost all microchannels have converged to the largest diameter is presented in Fig. 9d. The optimum individual with the highest void volume fraction (and consequently the minimum flow resistance) would have all its microchannels with the largest diameter, thus it is expected that running the algorithm for more generations or with a higher population size would produce this result. Note that having diagonal microchannels and the null diameter in the diagonal template optimization allows us to obtain individuals in a wider range for both objective functions and a much more efficient flow network for a given void volume fraction.

4.3. Effect of network minimum degree

We now turn our attention to the issue of coverage imposed as a constraint by requiring a minimum degree $\bar{d}$ on all vertices of the graph (Eq. (8)). It was shown in Section 2.3 how this parameter relates to the reliability of the network when subjected to damage. We vary the minimum degree target $\bar{d}$ from 0 (unconstrained case) to 3 (networks having at least three incident microchannels at each vertex) for networks within a 2D square domain with side $a = 10$ mm over a 6×6 point lattice ($\delta = 2$ mm). Refer to Fig. 2 for the template network used in the optimization and to Section 3.2 for a description on the reference network used for the normalization of the objective function values. For this study, the diameter set is $\mathscr{D}[\mu\text{m}] = \{0, 100\}$. Again, the inflow and outflow vertices are located at the lower-right and upper-left corners, respectively. The non-zero flow constraint is not imposed in all optimizations of this section.

Fig. 10 presents the resulting Pareto-optimal fronts for all optimizations. For high values of the void volume fraction, all curves lie on top of each other since the distinction between different values of $\bar{d}$ vanish for "fully populated networks". For low values of ϕ_v, notable differences are obtained, with low-$\bar{d}$ networks achieving better flow efficiencies. Some of the resulting networks, labeled (a) through (l) on the fronts, are also shown in Fig. 10. The first four figures correspond to the unconstrained case ($\bar{d} = 0$). The optimal solution for an individual containing the minimum void volume fraction would correspond to a set of microchannels forming a straight path between the source and the target. The network shown in Fig. 10a has a structure similar to that of the reference network used for normalization and the algorithm would have matched it had it been run for more generations or had the

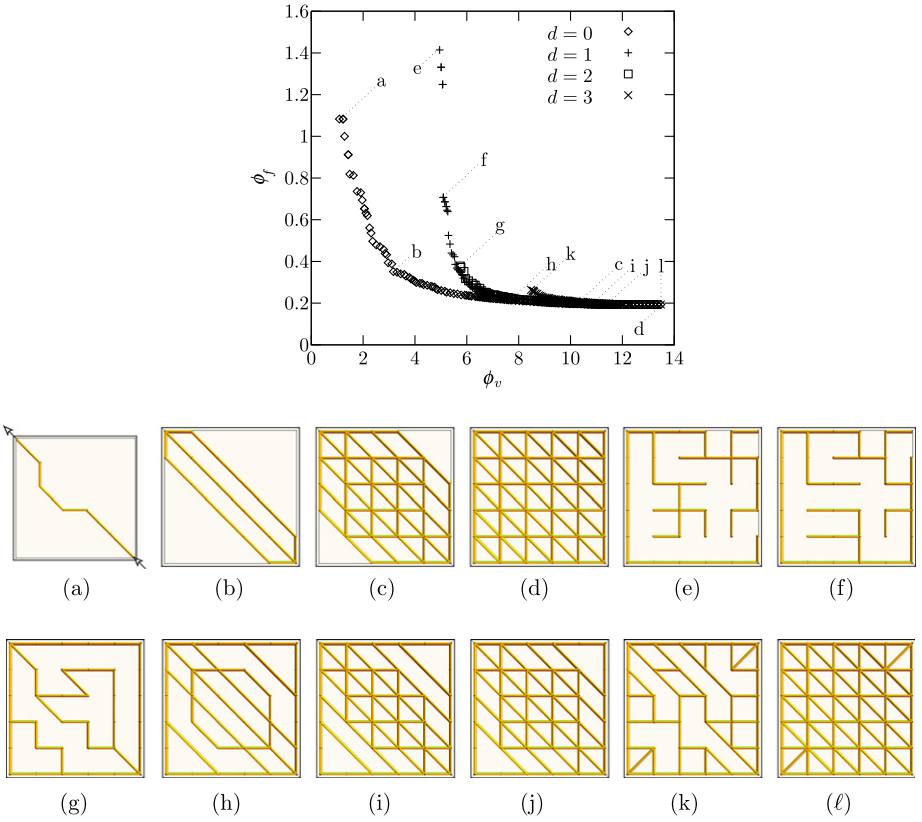

Fig. 10. NSGA-II results for network minimum degree study (top) and selected networks labeled (a) through (l) in the Pareto-optimal fronts. (a) through (d): $\bar{d} = 0$; (e) and (f): $\bar{d} = 1$; (g) through (j): $\bar{d} = 2$; (k) and (l): $\bar{d} = 3$. Source and target locations are marked by arrows in Fig. 10a.

population size been increased. The individual shown in Fig. 10d matches the optimum containing the highest void volume fraction. Note once again how the optimized networks naturally align with the source to target direction. Networks in Figs. 10b and c correspond to two individuals with intermediate objective function values. Structures in Figs. 10e and f belong to the second optimization, with imposed minimum degree $\bar{d} = 1$. The first network shows how the flow efficiency is deteriorated by maximizing the distance between inflow and outflow. The second network shows a jump in the pressure drop in Fig. 10 due to the fact that this is the first network for which the flow reaches the outflow in two distinct paths. The networks resulting from the optimization with an imposed degree $\bar{d} = 2$ are labeled Figs. 10g through j. The first network shows the individual with minimum void volume fraction. The next three individuals show symmetric patterns that result from the optimization in increasing order of void volume fraction. The last two figures, labeled Figs. 10k and l, illustrate the results for the last optimization for which $\bar{d} = 3$. Note that the algorithm has oriented the two microchannels in the lower-left and upper-right corners of the lattice in order to respect the constraint on the degree. These two networks correspond to the extreme point locations on the Pareto-optimal front for this optimization.

4.4. Diameter set study

The influence of the magnitude of one of the diameters in the set as it increases from $D = 20$ μm to $D = 80$ μm is studied in this section for diagonal networks. Thus, the ith optimization has a set of diameters $\mathscr{D}_i[\mu\text{m}] = \{0, 20(i-1), 100, i = 1, 2, \ldots, 5\}$. As in the previous case, the square domain for this problem has a side $a = 10$ mm, and spacing $\delta = 2$ mm. Also, let us consider as feasible only those networks with imposed degree $\bar{d} = 2$, which guarantees a complete coverage of the domain and same level of redundancy.

Once again, the results obtained from the algorithm are shown in Fig. 11, which are very similar to those given in the previous section since all curves lie on top of each other for high values of void volume fraction. The effect of the intermediate diameter value is seen for small values of ϕ_v. The figure was cropped for visualization purposes, as some networks composed almost exclusively of intermediate-diameter microchannels are characterized by very high pressure drop values. Recall that the pressure drop is inversely proportional to the fourth power of the diameter. The results presented in Fig. 11 indicate that the most efficient networks combine large-diameter microchannels directing most of the flow between the source and the target and small-diameter ones addressing the coverage and redundancy requirement, as is the case in many biological systems.

4.5. 3D optimization

A 3D domain is optimized in this section by simply changing the template structure. This can be done because the underlying optimization scheme using GAs is independent of the network used as the template. As usual, we take ϕ_v and ϕ_f as primary objective functions. Consider a cuboid with $a = b = c = 10$ mm (i.e., a cube) and a $11 \times 11 \times 11$ point lattice ($\delta = 1$ mm). The template and reference networks have the same structure and consist of microchannels oriented only in the directions of the coordinate axes x, y and z (i.e., orthogonal network). For this structure, there are $\mathscr{E} = 3n^2(n-1) = 3630$ edges, where $n = a/\delta + 1$. The diameter set considered is again $\mathscr{D}[\mu\text{m}] = \{0, 100, 200\}$ with a fixed diameter

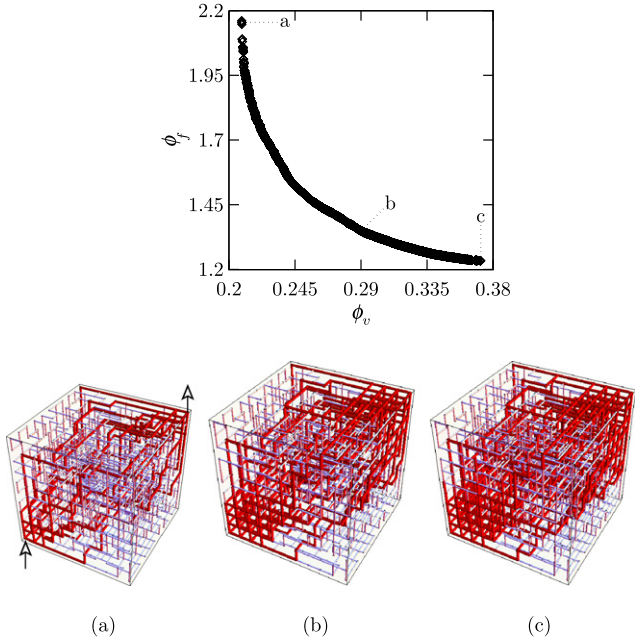

Fig. 12. NSGA-II results for a 3D optimization (top) and selected networks lying on the Pareto-optimal front (bottom). Darker-colored microchannels correspond to those with the largest diameter. The arrows in Fig. 12a show source and target locations.

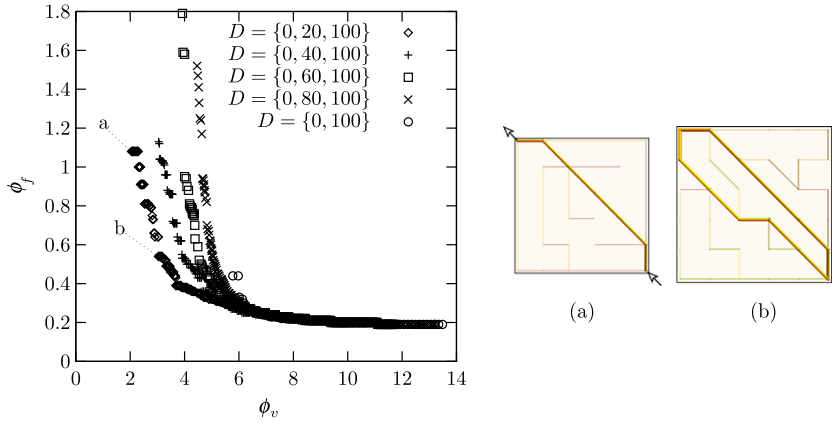

Fig. 11. NSGA-II results for the diameter set study. Networks labeled (a) and (b) are shown on the right and correspond to the optimization with diameter set $\mathscr{D}[\mu m] = \{0, 20, 100\}$. The source and target locations are marked as arrows in Fig. 11a.

for the reference structure $D_{\text{ref}} = 150$ μm, resulting in $v_{\text{ref}} = 7.63\%$. For this problem the inflow is located at one of the vertices of the cube and the outflow is located at the vertex furthest from the inflow. The optimization is constrained to those networks having non-zero flow in all microchannels and having a minimum degree $\bar{d} = 2$.

Results for this optimization are summarized in Fig. 12, where some structures lying on the optimal front (top) are selected for visualization (bottom). Darker-colored microchannels have the largest diameter value $D = 200$ μm. The results follow the same criteria described in the previous sections, where the emergence of sets of microchannels having the largest diameter reduce the pressure drop but increase the void volume fraction. It is worth mentioning that this problem has a total of 3^{3630} different networks and yet the trade-off between conflicting objective functions is still well captured with a relatively modest population size of 8000 individuals.

4.6. 3-objective optimization

A third objective function that deals with the homogeneity of flow at target locations is introduced here. Consider a 3D cuboid with dimensions $a = 10$ mm, $b = 4$ mm and $c = 1$ mm. A point lattice with $\delta = 1$ mm produces $11 \times 5 \times 2$ possible vertex locations. Furthermore, consider all vertices lying on the top surface of the cuboid as outflows (totalling $T = 55$ targets) and a single inflow is located at the midpoint of a short edge at the bottom surface. The template and reference network for this optimization are again orthogonal networks. The reference network has a diameter $D_{\text{ref}} = 50$ μm and the diameter set to consider is $\mathscr{D}[\mu\text{m}] = \{0, 10, 100\}$. The minimization problem is then

$$\begin{aligned} &\text{minimize} \quad \boldsymbol{\phi} = \{\phi_v, \phi_f, \phi_h\}, \\ &\text{such that} \quad \mathbf{g} = \{g_D, g_F\} = \mathbf{0}. \end{aligned}$$

For this problem the degree constraint is relaxed at outflow locations because failing to do so would always produce unfeasible networks. In other words, all outflow vertices have the same pressure so any microchannel connecting two of them would have had zero flow had the degree constraint been satisfied.

Two different views of the resulting "Pareto-optimal surface" are illustrated in Fig. 13, along with selected network structures. Once again the algorithm is able to capture the tradeoffs between the different objectives. After a few generations the algorithm eliminates all unfeasible solutions. This translates in assigning a zero diameter to all microchannels of the template close to the upper surface of the cuboid since all of them have zero flow. The network labeled Fig. 13a has the minimum value $\phi_h = 0.0005$ for the flow homogeneity objective function, showing that all vertical microchannels take the lowest non-zero diameter and a distribution network is created underneath. This network achieves a nearly optimum outflow distribution, with minimum and maximum outflow values deviating by only -1.25% and 1.46% respectively, from the optimum value $\dot{m}_S/T$. As shown in Fig. 13 (top), the optimal front has a distinct discrete nature and is composed of two main "branches". The solution labeled Fig. 13b belongs to a set of solutions where ϕ_h is not optimal. However, these solutions are characterized by a substantially better flow efficiency as one or more large-diameter microchannels link the source to at least one of the targets. Finally, the network Fig. 13c corresponds to the individual with the lowest void volume fraction for this particular run, showing most of the microchannels converged to the smallest non-zero diameter. However, this network is not as optimal as network Fig. 13a in terms of outflow uniformity ($\phi_h = 0.1053$) and pressure drop ($\phi_f = 203.1$).

5. Conclusions

This work has presented a study on the use of a multi-objective GA in the optimization of microvascular flow networks decomposed into a set of mathematically simple objective functions. The algorithm is able to capture adequately the tradeoff between conflicting objective functions and to eliminate unfeasible solutions. Constraints restrict the search space and guide the algorithm to obtain only feasible solutions after a few generations. The GA naturally evolves the networks towards paths of minimal flow resistance between the source and the target. The optimized results show how the addition of diagonal microchannels in the template improves flow efficiency, specially at low values of the void

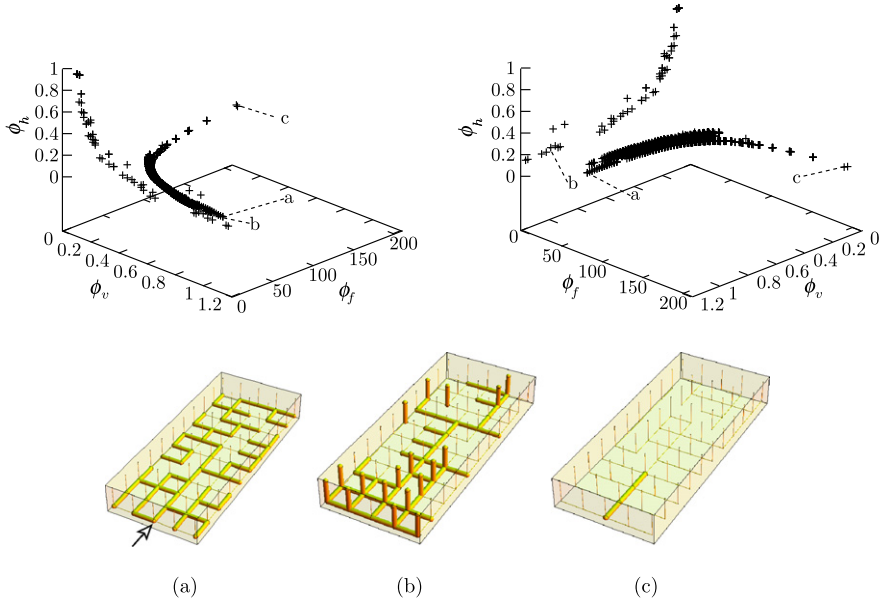

Fig. 13. NSGA-II results showing two different views of the Pareto-optimal surface for a 3-objective problem (top) and selected resulting structures (bottom). The boundary conditions for the flow objectives consider a single inflow shown by an arrow in Fig. 13a and 55 outflows located in the upper surface.

volume fraction. The analysis also demonstrated the cost in terms of void volume fraction of added redundancy in the networks. Similar to many biological systems, the most flow-efficient networks resulting from the GA optimization combine large-diameter microchannels directing most of the flow between the source and the target with small-diameter ones addressing the coverage and redundancy requirements. Even though the study was carried out on simple geometries, the extension to more complex geometries is easily accomplished by selecting a different template structure since the underlying evolution process is independent of the template selection, as demonstrated in the optimization of 3D templates.

To conclude this study, let us mention a couple of issues associated with the multi-objective GA used in this microvascular network design. In all problems studied in this work, the NSGA-II algorithm has no difficulty reaching the Pareto-optimal front and, once this front is reached, the subsequent generations create individuals that spread uniformly along it. However, the use of the crowding distance parameter in the selection exchanges optimal solutions in tightly crowded areas over the front for non-optimal yet less crowded ones [9]. Also, the algorithm has difficulties when trying to find the individuals with extreme values on the Pareto front. Furthermore, the algorithm does not scale well with the problem size. However, there have been successful attempts to obtain scalable GAs by combining the algorithm with other techniques [26] or by exploiting the "embarrassingly parallel" nature of the evaluation process [7].

Acknowledgements

A. Aragón, P. Geubelle and S. White gratefully acknowledge support from AFOSR (MURI Grant No. F49550-05-1-0346). J. Wayer's participation in the Undergraduate Research Opportunity Program was also supported by funds from the Illinois Space Grant Consortium and the Boeing Company. D. Goldberg's contribution to this work was sponsored by the AFOSR (Grant No. FA9550-06-1-0096).

References

[1] A.M. Aragón, C.J. Hansen, W. Wu, P.H. Geubelle, J.A. Lewis, S.R. White, Computational design and optimization of a biomimetic self-healing/cooling material, in: Proceedings of SPIE, vol. 6526, 2007.
[2] T. Bäck, H.-P. Schwefel, Evolution Strategies I: Variants and their Computational Implementation Chapter 6, John Wiley & Sons Limited, 1995. pp. 111–126.
[3] A. Bejan, S. Lorente, Constructal theory of generation of configuration in nature and engineering, J. Appl. Phys. 100 (4) (2006) 041301.
[4] A. Bejan, S. Lorente, K.-M. Wang, Networks of channels for self-healing composite materials, J. Appl. Phys. 100 (3) (2006) 033528.
[5] T. Borrvall, A. Klarbring, J. Petersson, B. Torstenfelt, Topology optimization in fluid mechanics, in: Fifth World Congress on Computational Mechanics, 2002.
[6] C.A. Brebbia, A.J. Ferrante, Computational Hydraulics, Butterworths, London, 1983.
[7] E. Cantú-Paz, D.E. Goldberg, Efficient parallel genetic algorithms: theory and practice, Comput. Methods Appl. Mech. Engrg. 186 (2000) 221–238.
[8] L. Davis (Ed.), Handbook of Genetic Algorithms, Van Nostrand Reinhold, 1991.
[9] K. Deb, Multi-Objective Optimization Using Evolutionary Algorithms, first ed., John Wiley & Sons Limited, 2001.
[10] K. Deb, S. Agrawal, A. Pratap, T. Meyarivan, A fast and elitist multiobjective genetic algorithm: NSGA-II, IEEE Transact. Evol. Comput. 6 (2) (2002) 181–197.
[11] J. Edmonds, R.M. Karp, Theoretical improvements in algorithmic efficiency for network flow problems, J. Assoc. Comput. Mach. 19 (2) (1972) 248–264.
[12] C.M. Fonseca, P.J. Fleming, Genetic algorithms for multiobjective optimization: formulation, discussion and generalization, in: S. Forrest (Ed.), Genetic Algorithms: Proceedings of the Fifth International Conference, Morgan Kaufmann, San Mateo, CA, 1993.
[13] R.T.G. Williams, I. Bond, A self-healing carbon fibre reinforced polymer for aerospace applications, Compos. Part A: Appl. Sci. Manufact. 38 (6) (2007) 1525–1532.
[14] D.E. Goldberg, Genetic Algorithms in Search, Optimization, and Machine Learning, Addison-Wesley Publishing Company, Masachusetts, 1989.
[15] D.E. Goldberg, The Design of Innovation: Lessons from and for Competent Genetic Algorithms, Kluwer Academic Publishers, Massachusetts, 2002.
[16] J.H. Holland, Outline for a logical theory of adaptive systems, J. Assoc. Comput. Mach. 9 (3) (1962) 297–314.
[17] J.H. Holland, Adaptation in Natural and Artificial Systems: an Introductory Analysis with Applications to Biology, Control, and Artificial Intelligence, University of Michigan Press, Ann Arbor, MI, 1975.
[18] J. Horn, N. Nafpliotis, D.E. Goldberg, A niched pareto genetic algorithm for multiobjective optimization, in: IEEE World Congress on Computational Intelligence. Proceedings of the First IEEE Conference on Evolutionary Computation, vol. 1, 1994.
[19] S. Kim, S. Lorente, A. Bejan, Vascularized materials: tree-shaped flow architectures matched canopy to canopy, J. Appl. Phys. 100 (6) (2006) 063525.
[20] A. Klarbring, J. Petersson, B. Torstenfelt, M. Karlsson, Topology optimization of flow networks, Comput. Methods Appl. Mech. Engrg. 192 (35–36) (2003) 3909–3932.
[21] S. Kukkonen, J. Lampinen, GDE3: the third evolution step of generalized differential evolution, in: The 2005 IEEE Congress on Evolutionary Computation, vol. 1, 2005.
[22] S.V. Kumar, T.A. Doby, J.J.W. Baugh, E.D. Brill, S.R. Ranjithan, Optimal design of redundant water distribution networks using a cluster of workstations, J. Water Resour. Plan. Manage. 132 (5) (2006) 374–384.
[23] J.W.C. Pang, I.P. Bond, A hollow fibre reinforced polymer composite encompassing self-healing and enhanced damage visibility, Compos. Sci. Technol. 65 (11–12) (2005) 1791–1799.
[24] C.H. Papadimitriou, K. Steiglitz, Combinatorial Optimization: Algorithms and Complexity, Dover Publications, 1998.
[25] V. Pareto, Manuale di Economia Politica, Piccola Biblioteca Scientifica, Milan, 1906, translated into English by Ann S. Schwier (1971), Manual of Political Economy, MacMillan, London.
[26] M. Pelikan, K. Sastry, D.E. Goldberg, Multiobjective HBOA, clustering, and scalability, in: GECCO'05: Proceedings of the 2005 Conference on Genetic and evolutionary computation, ACM, New York, NY, USA, 2005.
[27] T.D. Prasad, N. Park, Multiobjective genetic algorithms for design of water distribution networks, J. Water Resour. Plan. Manage. 130 (1) (2004) 73–82.
[28] J.T. Richardson, M.R. Palmer, G.E. Liepins, M. Hilliard, Some guidelines for genetic algorithms with penalty functions, in: Proceedings of the third international conference on Genetic algorithms, Morgan Kaufmann Publishers Inc., San Francisco, CA, USA, 1989.
[29] H.-P. Schwefel, T. Bäck, Evolution Strategies II: Theoretical Aspects Chapter 7, John Wiley & Sons Limited, 1995. pp. 127–140.
[30] L.A. Shipton, Thermal management applications for microvascular systems, Master's thesis, University of Illinois at Urbana-Champaign, 2007.
[31] A.R. Simpson, G.C. Dandy, L.J. Murphy, Genetic algorithms compared to other techniques for pipe optimization, J. Water Resour. Plan. Manage. 120 (4) (1994) 423–443.
[32] N. Srinivas, K. Deb, Multiobjective function optimization using nondominated sorting genetic algorithms, Evol. Comput. J. 2 (3) (1995) 221–248.
[33] K. Steiglitz, P. Weiner, D. Kleitman, The design of minimum-cost survivable networks, circuits and systems, IEEE Trans. [legacy, pre - 1988] 16 (4) (1969) 455–460.
[34] D. Therriault, S.R. White, J.A. Lewis, Chaotic mixing in three-dimensional microvascular networks fabricated by direct-write assembly, Nat. Mater. 2 (4) (2003) 265–271.
[35] K.S. Toohey, N.R. Sottos, J.A. Lewis, J.S. Moore, S.R. White, Self-healing materials with microvascular networks, Nat. Mater. 6 (2007) 581–585.
[36] K. Vairavamoorthy, M. Ali, Optimal design of water distribution systems using genetic algorithms, Comput-Aided Civil Infrastruct. Engrg. 15 (5) (2000) 374–382.
[37] D.B. West, Introduction to Graph Theory, second ed., Prentice Hall, 2001.
[38] W. Wu, C.J. Hansen, A.M. Aragón, N.R. Sottos, S.R. White, P.H. Geubelle, J.A. Lewis, Direct ink writing of microvascular networks, in: Proceedings of the First International Conference on Self Healing Materials, Noordwijk aan Zee, The Netherlands, 2007.
[39] H. Zhang, S. Lorente, A. Bejan, Vascularization with trees that alternate with upside-down trees, J. Appl. Phys. 101 (9) (2007) 094904.